Annual Progress Report to the
Air Force Office of Scientific Research (AFOSR)

Advanced Photonic Crystal-Based Integrated Structures for Optical Communications and Optical Signal Processing

Georgia Institute of Technology

Principal Investigator:

Ali Adibi
Associate Professor, School of Electrical and Computer Engineering,
Georgia Institute of Technology
Atlanta, GA 30332-0250
e-mail:adibi@ee.gatech.edu
Tel: (404) 385-2738
Fax: (404) 894-4641

REPORT DOCUMENTATION PAGE

Form Approved
OMB No. 0704-0188

1. REPORT DATE *(DD-MM-YYYY)*	2. REPORT TYPE	3. DATES COVERED *(From - To)*
22-11-2010	Final Technical	01-MAR-2007 to 30-APR-2010

4. TITLE AND SUBTITLE
ADVANCED PHOTONIC CRYSTAL-BASED INTEGRATED STRUCTURES FOR OPTICAL COMMUNICATIONS AND OPTICAL SIGNAL PROCESSING

5a. CONTRACT NUMBER

5b. GRANT NUMBER
FA9550-07-1-0201

5c. PROGRAM ELEMENT NUMBER

6. AUTHOR(S)
Ali Adibi

5d. PROJECT NUMBER

5e. TASK NUMBER

5f. WORK UNIT NUMBER

7. PERFORMING ORGANIZATION NAME(S) AND ADDRESS(ES)
Georgia Tech

8. PERFORMING ORGANIZATION REPORT NUMBER
4

9. SPONSORING/MONITORING AGENCY NAME(S) AND ADDRESS(ES)
AFOSR-RSE
875 N. Randolph St. STE 325 RM 3112
Arlington VA 22203

10. SPONSOR/MONITOR'S ACRONYM(S)
AFOSR-RSE

11. SPONSOR/MONITOR'S REPORT NUMBER(S)
AFRL-OSR-VA-TR-2012-0180

12. DISTRIBUTION/AVAILABILITY STATEMENT
Distribution A

13. SUPPLEMENTARY NOTES

14. ABSTRACT
This AFOSR-supported research was directed toward realizing low-loss large-bandwidth guiding and processing units based on photonic crystals in an integrated level. To achieve this goal, in what follows, different steps (including efficient guiding of light through the planar platform, efficient demultiplexing, methods to flawlessly putting devices together, and actual demonstration of functionalities) to realize this integrated platform will be discussed. Our research in this field has resulted in a large number of scientific publications and technical presentations.

15. SUBJECT TERMS
Photonic Crystal, Optical Signal Processing, Photonics, Integrated Circuits, Integrated Structures

16. SECURITY CLASSIFICATION OF:			17. LIMITATION OF ABSTRACT	18. NUMBER OF PAGES	19a. NAME OF RESPONSIBLE PERSON
a. REPORT	b. ABSTRACT	c. THIS PAGE			Ali Adibi
					19b. TELEPHONE NUMBER *(Include area code)*
U	U	U	UU	19	4043852738

I. Introduction

This final report summarizes achievements in Dr. Adibi's research group at Georgia Institute of Technology in the area of chip-scale WDM devices using photonic crystals supported by Air Force Office of Scientific research (AFOSR) during the course of this program. Only major achievements with brief descriptions are listed in this report. Detailed information can be found in the recent publications or can be directly requested from Dr. Adibi.

This AFOSR-supported research was directed toward realizing low-loss large-bandwidth guiding and processing units based on photonic crystals in an integrated level. To achieve this goal, in what follows, different steps (including efficient guiding of light through the planar platform, efficient demultiplexing, methods to flawlessly putting devices together, and actual demonstration of functionalities) to realize this integrated platform will be discussed. Our research in this field has resulted in a large number of scientific publications and technical presentations. A complete list of journal papers and conference presentations is included at the end of this report. AFOSR support has been acknowledged in all these publications and presentations.

II. Research Accomplishments

II.A Enhancing the guiding bandwidth of photonic crystal waveguides on SOI

In the first two years of this program, we proposed that the dispersion of a photonic crystal waveguide (PCW) can be engineered by appropriate modification of the size or periodicity of the air holes close to the guiding region. The former perturbation resulted in single mode guiding and the latter in elimination of the modegap, dispersion linearization, and loss reduction. Knowing the individual roles of the hole size (r') and periodicity of holes (a') in the rows next to the guiding region on the properties of PCWs, it is essential to allow both parameters (or degrees of freedom) to vary simultaneously for a more careful optimization of PCWs. This task was done during the last year of the program. Figure 1 shows a scanning electron microscopy (SEM) image of these structures with definitions of the radii and the period of the air holes close to the guiding region.

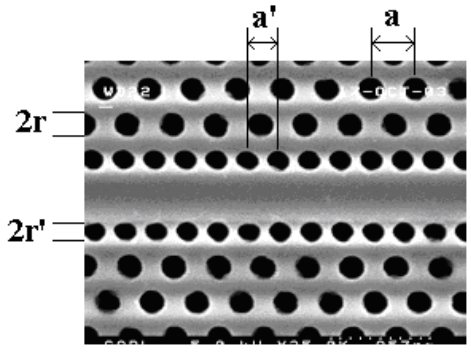

Figure 1. SEM view of a biperiodic photonic crystal waveguide is shown. The radius and the period of the air holes in the two rows next to the guiding region are a'=0.7a and r'=0.25a, respectively, and the lattice constant is a=420nm.

In this work, we present a systematic approach for improving the guiding bandwidth of a PCW in an SOI platform while keeping the periodicity of the PC. This is achieved by engineering the holes

in the second row of the PCW above and below the main guiding region as a result of the reduction of the interaction of the low-group-velocity fundamental mode near the Brillouin's zone edge with the surrounding PC. We show that by decreasing the sizes of the holes in the second row from 240 nm to 120 nm the guiding bandwidth is increased from 2.5 nm to 12 nm.

We consider a triangular lattice PC of air-holes on an SOI substrate, which provides a large photonic bandgap for the TE-like polarized light. Figure 1(a) shows the structure of a W1 PCW created by removing one row of holes along the ΓK direction of this PC lattice. The dispersion of this PCW with radius of all air holes $r_1 = r_2 = 0.3a$ (a is the lattice constant of PC) is simulated using an effective refractive index of $n_{eff} = 2.84$ with two-dimensional plane-wave-expansion method and is shown in Fig. 1(b) by the curves with circle markers. Solid curves show the dispersion of guided modes with even symmetry, which are of great practical interest, and dotted curves show the dispersion of the guided modes with odd symmetry. Light-line of SiO_2 substrate is also shown by the dashed line and the continuums of TE-like and TM-like modes are illustrated by the dark and light gray regions in Fig. 1(b), respectively. Because of the asymmetry of the device in the lateral direction (different substrate and cladding materials), TE-like guided modes which overlap with the continuum of TM-like modes of the bulk PC interact (or couple) with them; and thus, can leak into the surrounding PC. As it is observed in Fig. 1(b) the portion of the dispersion curve below the TM-like modes of the PC has lower group velocity compared to the leaky linear portion of the dispersion which is above the TM-like mode and this leads to a small low-loss guiding bandwidth. This behavior is concurrent with the larger field distribution of LGV modes compared to that of high group velocity (HGV) linear modes and consequently more interaction with the surrounding PC. This behavior is shown in insets *E1* and *E2* where they depict the distribution of the H_z field component of the even mode at normalized propagation constants ($\beta a/2\pi$) of 0.25 and 0.5, respectively. Thus, modifying the PC structure in the second row of holes will primarily affect the even mode in the LGV region (e.g., *E2* mode), while having minimal effect in the linear portions of the dispersion diagram (e.g., *E1* mode). By reducing r_2, we increase the effective index of the guided mode resulting in a downward (or red) shift of its dispersion diagram at LGV region which results in more guiding bandwidth. We calculated the PCW dispersion with different values of r_2 in Fig. 1(a), and results are shown in Fig. 1(b). Curves with square and diamond markers in Fig. 1(b) represent the dispersion of W1 PCW for $r_2 = 0.25a$ and $r_2 = 0.2a$, respectively. As observed in Fig. 1(b), HGV modes are not perturbed considerably with reducing r_2, while LGV modes are shifted to lower frequencies, and consequently, the bandwidth of the waveguide is increased.

In order to confirm the simulation results, we fabricated these waveguides on an SOI wafer with Si thickness of 250 nm and buried oxide thickness of 1 μm. The lattice constant of the PC is 400 nm and tapered ridge waveguides are used to couple light in to PCW. Figure 2(b) shows a scanning electron micrograph of the fabricated device at the interface of the input ridge waveguide and the PCW. Characterization of the transmission spectrum of the fabricated PCWs is done by coupling a collimated beam from a tunable laser into the input ridge waveguide and measuring the output signal power from the output ridge waveguide by a photodetector. Figure 2 shows the transmission spectra of three PCWs with different radii of the second layer holes (r_2 = 120 nm, 100 nm, and 80nm). The radii of all the other holes are 120 nm. It is obvious from the measured transmission spectra that the guiding bandwidth is enhanced by reducing the radius of the second layer of air-

holes. This bandwidth is 2.5 nm, 7 nm and 12 nm for r_2 = 120 nm, 100 nm, and 80nm, respectively. The low-loss guiding bandwidths of these PCWs are simulated by the three-dimensional (3D) FDTD method and are shown by bars in Fig. 2 on top of the transmission spectra.

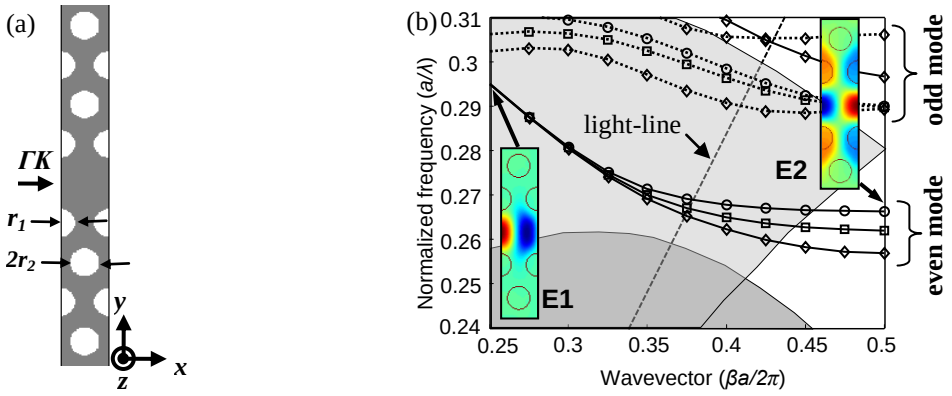

Figure 1. (a) Structure of a W1 PCW in the plane of PC; the lattice constant is a, the radius of holes in the second row above and below the guiding region is r_2, and the radius of the other modes is r_1 (b) Dispersion diagrams of W1 PCWs with r=0.3a and effective index of n_{eff} =2.84. Circle, square and diamond markers represent PCW with the normalized radius of the second layer holes r_2=0.3a, r_2=0.25a and r_2=0.2a, respectively. Solid and dotted curves represent modes with even and odd symmetries, respectively. Dashed line is the light-line of SiO_2 substrate. Dark and light gray regions represent the continuum of the bulk PC modes with TE-like and TM-like polarizations, respectively. Insets *E1* and *E2* show the profile of the H_z field of W1 PCW with r_2=0.3a at normalized propagation constants ($\beta a/2\pi$) of 0.25 and 0.5, respectively.

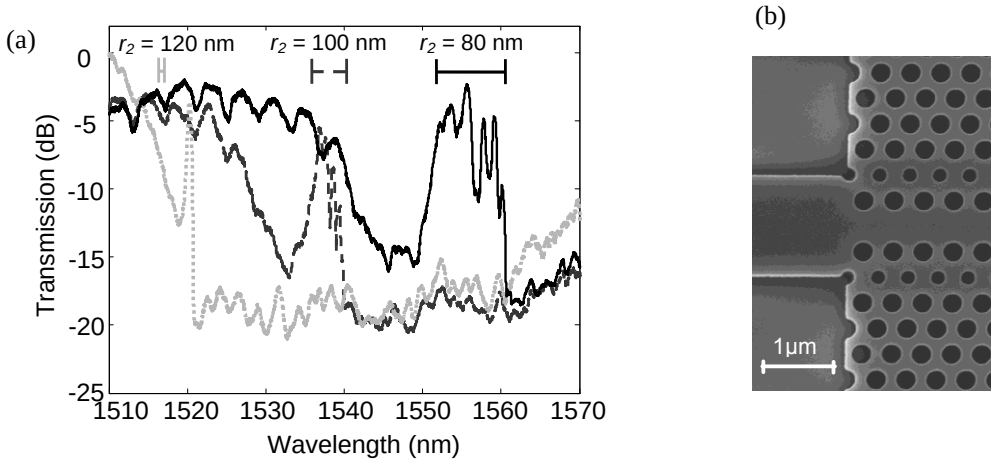

Figure 2. Transmission spectra of W1 PCWs fabricated on SOI with the silicon thickness of 250 nm with a=400 nm and r_1= 0.3a = 120 nm. The transmission spectrum for PCWs with r_2 = 120 nm, r_2 = 100 nm and r_2 = 80 nm are measured and shown by dotted, dashed and solid curves, respectively. (b) Scanning electron micrograph of the fabricated device at the interface of the input ridge to PCW.

In order to analyze the features in the transmission spectrum in detail, the dispersion diagram simulated using the 3D FDTD method and the transmission spectrum of the PCW with r_2 = 80 nm are plotted side-by-side in Figs. 3(a) and 3(b), respectively. Dispersion curves of guided modes with even and odd symmetries are shown in solid and dotted curves in Fig. 3(a), respectively. By comparing Figs. 3(a) and 3(b), it is observed that the leaky modes of the PCW coincide with the

continuum of the TM-like bulk modes of the surrounding PC. Another important feature of the dispersion of the even mode of this PCW is the presence of a mode-gap in the low-loss portion of its dispersion (and transmission). This gap is formed by the coupling of contra-propagating TE-like (TE^E) and TM-like (TM^E) guided modes with even symmetry. "E" and "O" superscripts indicate the even and odd symmetry of the mode, respectively. TE^E is the guided mode of interest and TM^E is a donor mode separated from the continuum of TM-like modes of the PC through the defect introduced in the second row holes around the guiding region. Combining our theoretical and experimental results in this work, we can conclude that the reduction of the second row hole radius from $r_2 = 0.3a$ to $r_2 = 0.2a$ can improve the guiding bandwidth from a negligible value of 2.5 nm to a more practical value of 12 nm. We also elaborated on the presence of a mode-gap in the transmission spectrum.

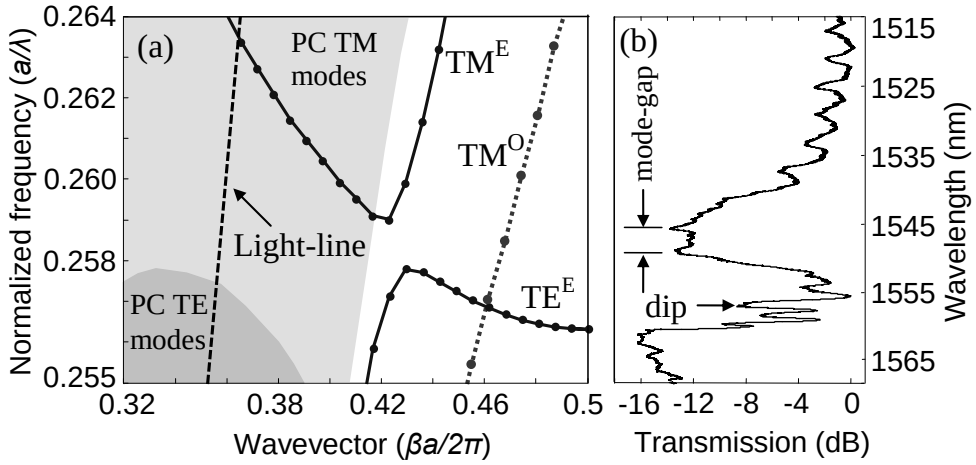

Figure 3. (a) Dispersion diagram of W1 PCW on SOI wafer with Si thickness of 250 nm, a=400nm, r_1 = 120 nm, and r_2 = 80 nm. Dark grey and light grey regions represent the continuum of TE-like and TM-like PC bulk modes, respectively; dashed line is the light-line of the substrate, solid and dotted curves are dispersion curves of guided modes with even and odd symmetries (within the plane of PC), respectively. (b) Transmission spectrum of the PCW described in (a).

II.B Adiabatic couplers for efficient injection of light into slow group velocity modes of PCW

Photonic Crystal waveguides differ from conventional ridge waveguides in the sense that due to the periodicity in the guiding direction they support low group velocity modes. These low group velocity modes offer characteristics such as dispersion and large light matter interaction which can be used to design much more compact devices for use in dispersion compensation, delay line and non-linear applications. Unfortunately, coupling light into these low group velocity modes is not easy and suffers from large insertion loss. The larger the group velocities mismatch between the ridge waveguide and PCW the larger the insertion loss. We have designed Ridge-PCW Couplers that offer flat transmission throughout the frequency range of interest irrespective of the group velocity.

Previously we reported our simulation work of achieving group velocity insensitive coupling of electromagnetic energy from a ridge waveguide to a PCW. Two different designs were reported: i) taper coupler in which either the air hole radius or the period of the PCW is tapered to allow light

to transform from high group velocity modes to low group velocity modes, and ii) air wedge coupler in which the ridge waveguide modes are directly transformed into PCW modes by modifying the structure in the evanescent field region from a ridge waveguide to a PCW. Here we report the experimental results of our designed couplers and compare these with a simple butt coupler. Figure 4 shows the SEM images of the fabricated PCWs with a butt coupler and an air wedge coupler.

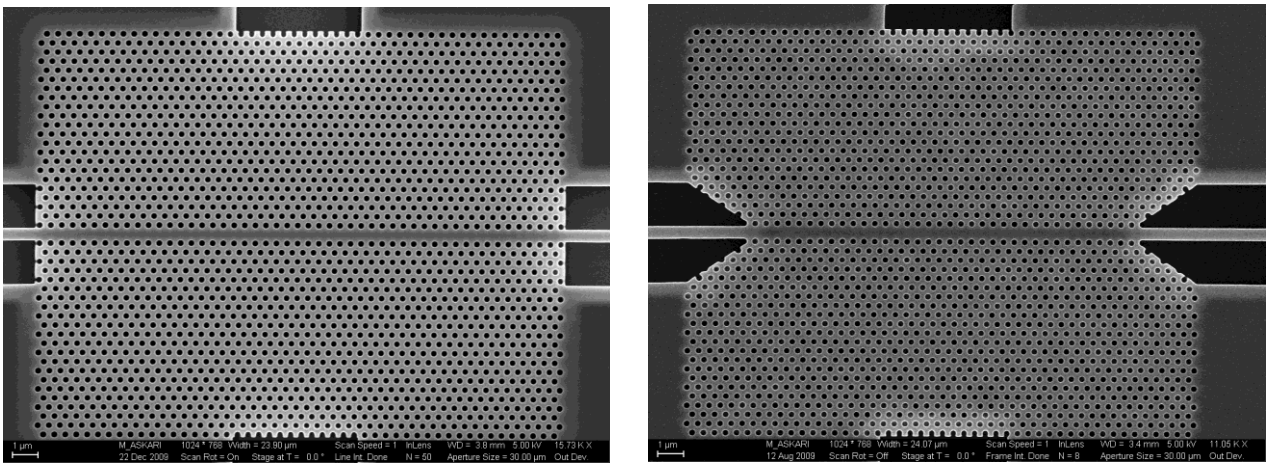

Figure 4. SEM image of fabricated butt coupler (left) and air wedge coupler (right).

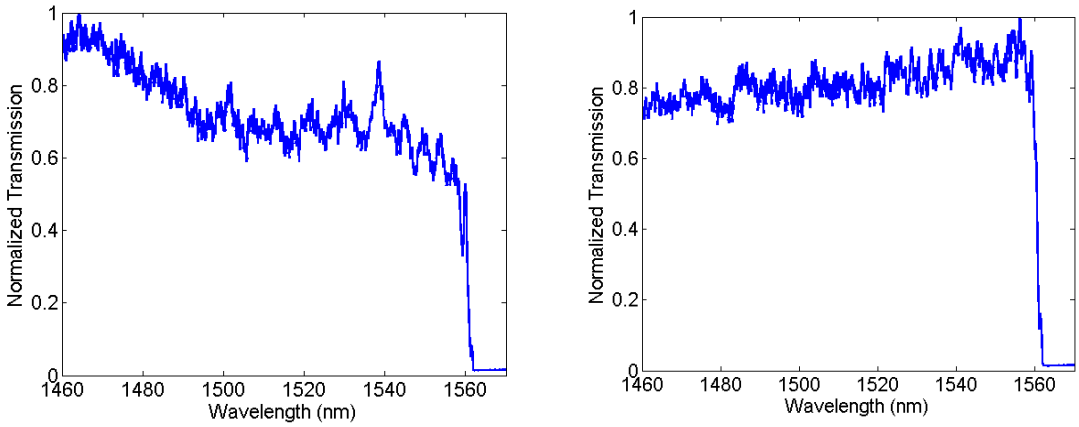

Figure 5. Characterization results of fabricated butt coupler (left) and an air wedge coupler (right).

Figure 5 shows the characterization results for the fabricated butt coupled PCW and an air wedge coupled PCW. The shape of the transmission for the air wedge coupler case is flatter, which shows that this coupler allows coupling more light into low group velocity modes of the PCW than the butt coupler case. We are in the process of writing a journal paper on our findings. A couple of conference presentations have already been delivered on our work.

II.C Wavelength demultiplexers based on preconditioned superprism effect in photonic crystals

Wavelength demultiplexing (WD) devices disperse an input beam into a plurality of sub-beams, and are commonly used to separate optical channels at different wavelengths. Compact WD devices are of great interest for several integrated photonic applications including optical information processing, optical communications and networking, as well as integrated optical sensing such as lab-on-a-chip biosensing systems. The compactness of these devices and their compatibility with integrated photonic and electronic platforms are among their main advantages when compared to other wavelength demultiplexing solutions. These advantages are the result of the wide range of controllable dispersive properties in a very compact structure enabled by the use of photonic crystals (PCs). Such dispersive properties are not available in conventional devices that usually rely on bulk or grating-based materials.

In order to realize an efficient WD device, in addition to a compact WD mechanism to achieve spatial separation of different wavelength channels, special measures must be taken to achieve high isolation from unwanted wavelength channels. The basic demultiplexing function can be obtained using the superprism effect in PCs, as shown in Figure 6(a). Due to the superprism effect, different wavelength channels inside the PC region propagate in different directions (determined by the direction of group velocity of the corresponding PC mode at each wavelength). Propagation in such a medium can eventually result in separation of different wavelength channels, but it has been shown that the diffraction of the optical beam at each wavelength channel results in broadening of the beam, which requires relatively large propagation length to achieve spatial separation with the required cross-talk level between adjacent wavelength channels. Recently, it has been theoretically proposed that compact demultiplexers at high resolutions can be realized by combining the superprism effect and negative diffraction. In these structures, the broadening of the beam due to normal diffraction effects is compensated by propagation in a PC region with negative diffraction, as shown in Figure 6(b). As a result of such diffraction compensation, the size of the beam at the output of these structures is reduced to approximately the transfer-limited beamwidth, and much smaller propagation lengths are required for spatial separation of adjacent wavelength channels. Another unique property of PCs is the negative refraction at their interface, as shown in Figure 6(c). In this case, the desired signal is refracted away from the direction of the incident signal, resulting in the separation of the desired signal from the stray signals.

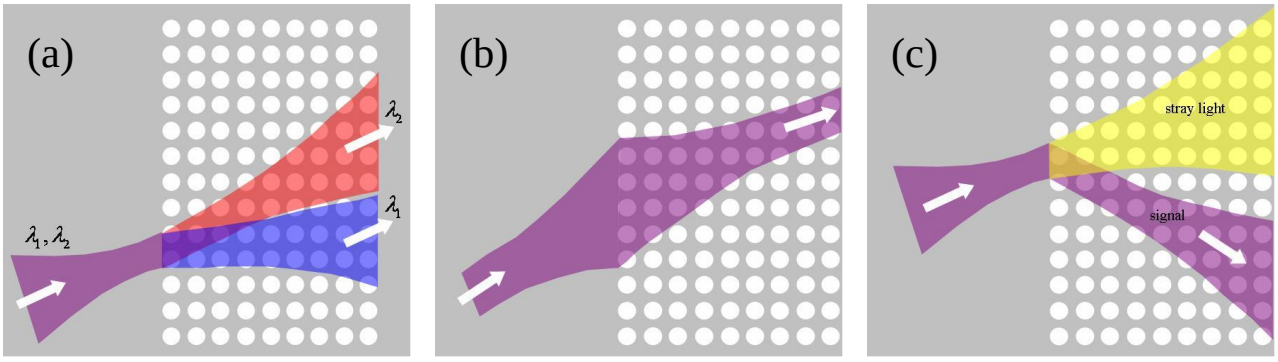

Figure 6. Three dispersive properties of PCs are schematically visualized: (a) the superprism effect, (b) the negative diffraction effect, and (c) the negative refraction effect.

We have already shown (*Optics Express*, 14, 2413, 2006) that it is possible to combine several unique dispersive properties of PCs for a desired application by optimizing the PC geometry (i.e., size and periodicity of the holes). In particular, we show that it is possible to engineer the modes of the PC to simultaneously have the three aforementioned dispersive properties (i.e., superprism effect, negative diffraction, and negative refraction) at the frequency range of interest. By combining these three properties, it is possible to realize compact and efficient PC demultiplexers. By such optimal dispersion engineering in PC devices, it is possible to simultaneously focus the separated channels down to a small size while propagating through the PC and divert the separated channels from the stray and unwanted signals. These considerable improvements are obtained without adding to the complexity of fabrication or requiring any special material growth. This is a main advantage of PCs in which a wide range of material properties can be achieved by simply modifying the geometry of air holes.

The resolution of currently demonstrated PC-based WD devices is not enough for demanding high-resolution optical communication and photonic information processing applications. To improve this resolution, we proposed to use higher photonic bands of the photonic crystals, which have stronger dispersive properties and are reported in the next section. In order to have WD devices compatible with the currently available integrated optical platforms, we will still choose the planar PC implementation on a silicon-on-insulator platform. Figure 7(a) shows an example of band structure of the second band of a square lattice photonic crystal in SOI, and Figure 4(b) shows the angular dispersion inside such a photonic crystal for an incident beam coming from the unpatterned slab region at a fixed angle. From Figure 7(b) it can be observed that the angle of group velocity of the excited PC modes (i.e., the angle of propagation of corresponding optical beams) in this case varies rapidly with respect to the wavelength of the incoming beam. This rate of change is at least one order of magnitude larger than the response in the first photonic band, and at least two orders of magnitude larger than the response in a basic grating-based demultiplexer. Furthermore, by moving the operation point to higher photonic bands, the normalized frequency of operation (i.e., a/λ) becomes larger, and therefore, at a fixed operation wavelength of operation (e.g., 1550 nm), the feature sizes of structure become larger. This means that the fabrication constraints are more relaxed.

II.D Wavelength demultiplexers in higher photonic bands of planar photonic crystals

Wavelength demultiplexing (WD) is one of the major applications of unique dispersion properties of the PCs. Possibility of integration and compactness are two main advantages of PC based demultiplexers compared to other demultiplexing techniques for applications including compact spectrometers (for sensing applications) and WDM demultiplexers. Proof-of-concept demonstrations of this phenomenon have been performed in planar structures. However, the resolution of the demonstrated devices was not high enough to address the current demands of WDM applications. We have extended our previous idea of combining diffraction compensation with the superprism effect and have designed wavelength demultiplexing devices that are more compact (by an order of magnitude) and higher resolution compared to all previous demonstrations. This enhancement is achieved by using modes of the planar PC in their higher photonic bands (where dispersive effects are much stronger than the first band).

To develop a new application using the dispersive properties of photonic crystals, an intuitive model to describe the (temporal and spatial) dispersion effects is needed. We have used the

envelope transfer function model (developed previously in this research) to analyze the beam propagation effects inside these periodic structures and have shown that it will provide a simple and insightful way to explore the dispersive properties. Another important step to pave the way for implementing more complex dispersive functionalities is to develop the capability of having multiple stages in the system. This process requires the fabrication of these devices to be further improved to reliably produce the designed structures. In addition, the insertion loss (from reflection and scattering) needs to be reduced and the compatibility issues need to be resolved to enable systematic implementation of such multi-stage systems.

The photonic crystal lattice designed for this purpose and its corresponding band structure for the second H-polarized band are shown in Figure 8(b). In this case, the photonic crystal consists of a square lattice array of circular holes, with a = 476 nm and r/a = 0.30. The effective index of the material in the photonic crystal region is chosen to be 2.68 to approximately model the planar structure. Similar to the previous case, the loci of modes excited inside the photonic crystal at the designed operation incident angle of α = 29° is shown as a red dotted curve in Figure 8(b). The output beam envelope profiles at different wavelengths at the output plane of this photonic crystal are shown in Figure 8(c). The overall configuration is similar to the one in Figure 8(a), with L = 50 μm, L_p = 1050 μm, $2w_0$ = 24 μm.

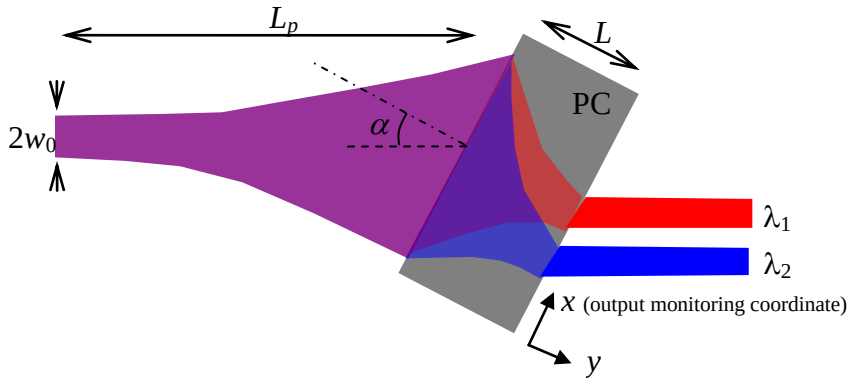

(a)

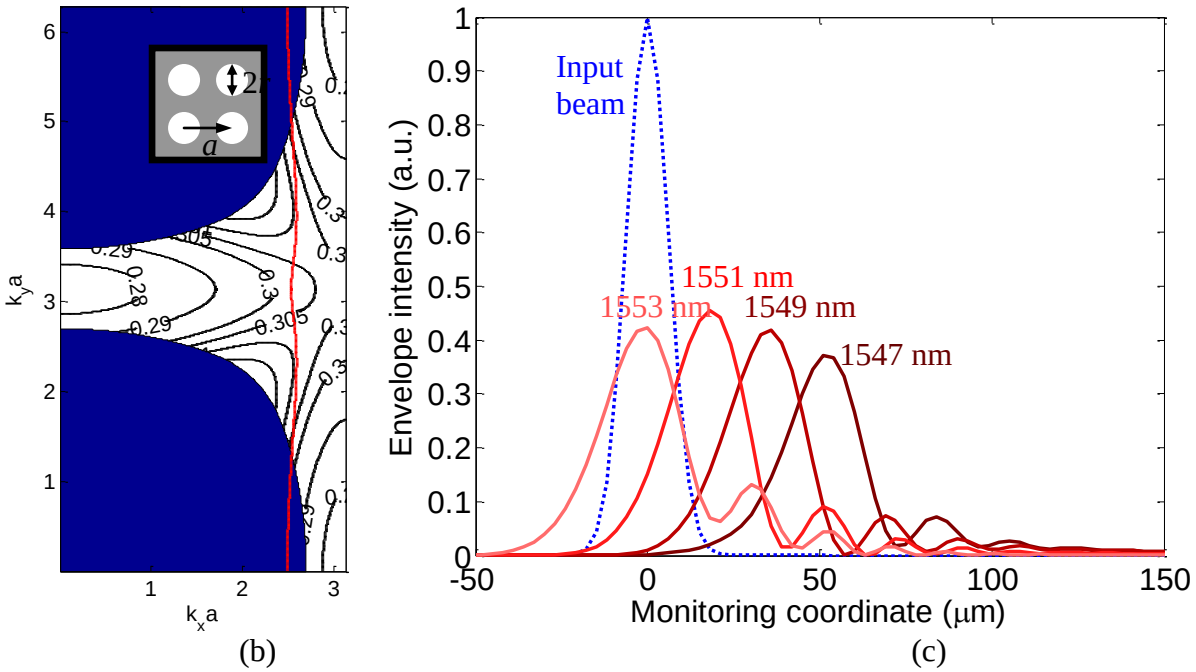

Figure 8. (a) Overview of a two-stage device for wavelength demultiplexing using the superprism effect in photonic crystals is schematically demonstrated. (b) Band structure of a photonic crystal structure (with a unit cell shown in the inset) is depicted in the form of iso-frequency contours. The corresponding normalized frequencies (a/λ) are marked on each contour. The red curve shows the loci of photonic crystal modes excited in this lattice by a plane wave coming at incident angle $\alpha = 29°$ at different wavelengths. The shaded region is above the light line in a planar implementation. (c) Beam profiles at the output interface of the photonic crystal region are shown at four wavelengths with 2 nm wavelength spacing.

To test the possibility of forming practical PC demultiplexers using the second band PC modes, we have designed a compact preconditioned PC demultiplexer to have the superprism effect, negative diffraction, and negative refraction simultaneously. We have fabricated the designed square lattice PC structure using electron beam lithography and dry etching on an SOI wafer. The PC structure has a lattice constant a = 400 nm and holes with a normalized radius r/a = 0.24. The lattice constant in the PC buffer stage is a = 200 nm, and the holes in the buffer region have a normalized radius of r/a = 0.30. The SEM image of the fabricated structure is shown in Figure 9. Figure 9(a) shows the close-up of the PC structure with buffer stage at the interfaces with Si, while Figure 9(b) shows the output waveguide array fabricated to sample the output signal of the PC demultiplexer. These output waveguides are 3 μm apart and are tapered down from a 2.7 μm width at the sampling point to 1 μm at the edge of the sample; thus, there is negligible cross-coupling between them. In this demultiplexer, the input beam (with a beam waist of 6 μm) is broadened initially by propagation through an unpatterned Si slab region [on the left in Figure 9(a)], such that after propagation through the PC structure (which is designed to have negative diffraction at the operation point) the beam is focused close to its diffraction-limited spot size at the output. This output beam profile is sampled by an array of waveguides spaced 3 μm apart and carried to the output edge of the sample, as shown in Figure9(b).

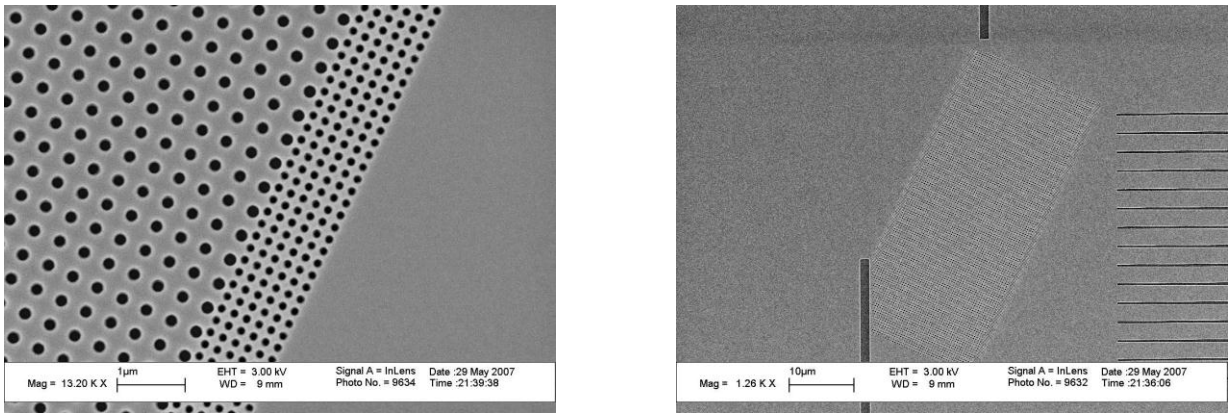

(a) (b)

Figure 9. (a) SEM image of the interface of the PC demultiplexer is shown, revealing the details of the PC buffer stage. (b) Overall view of the photonic crystal device is shown. Six layers of small-period buffer PC are used at each interface to avoid unwanted Floquet-type transmission and reflection orders. The waveguides on the right (which are spaced 3 μm apart) sample the output optical beam profile and carry the signal to the output edge of the SOI device.

To measure the response of the system, light from a tunable laser is coupled to the structure through an input waveguide, and transmission through each of the output waveguides in the output array is measured using a standard lock-in technique as the input wavelength changes. The results of such measurements for four of the output waveguides are shown in Figure 10(a). The wavelength at which the maximum transmission occurs for each of the output waveguides is the wavelength at which the beam is steered inside the PC structure towards that specific waveguide. The theoretical estimate of the refraction angles (i.e., the angle of group velocity inside the photonic crystal structure) and those measured in the experiment are plotted in Figure 10(b). The observations from the experiment confirm the operation of the PC structure in the negative refraction regime and demonstrate strong angular dispersion factor (~4°/nm) close to what is predicted by theoretical estimates. Note that the experimental plot shows the location of the peak of the output beam profile as a function of wavelength. Since this output beam profile is affected by higher-order diffraction effects, the location of the peak is different from the theoretical prediction of the angular dispersion (which relies only on the first-order effect). This fact causes the difference between the theoretical and experimental plots in Figure 10(b).

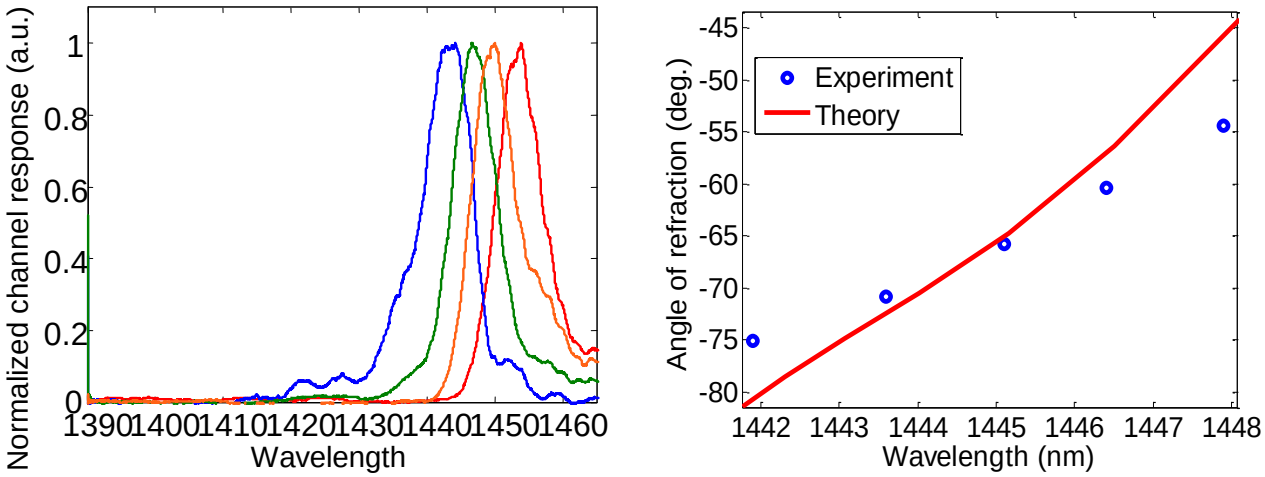

Figure 10. (a) Channel responses for four of the output waveguides in the structure shown in Figure 9 are measured and plotted after normalization. The wavelength of maximum transmission in each channel response presents the angle of refraction inside the PC corresponding to that wavelength. Plots of refraction angles inside the PC are plotted for different wavelengths using the experimentally measured transmission data (circles) and compared with those predicted from the band structure (solid curve).

We have addressed practical issues to be overcome for efficient demonstration of strong angular dispersion in a planar photonic crystal structure. We showed that by using dispersive properties of the second photonic band of a square lattice PC in an SOI wafer, strong angular dispersion (~4°/nm change in the refraction angle in a negative refraction regime) can be achieved. We also showed that the unwanted reflection and diffraction effects caused by operation at higher photonic bands can be avoided by designing a PC buffer stage. Using a simple design, we demonstrate a 20 μm × 50 μm PC demultiplexer with 3 nm resolution an at least 2.4 dB cross-talk isolation. These performance measures can be improved considerably by optimizing the PC demultiplexer. We believe that the results achieved in this research can be used for designing compact PC demultiplexers and spectrometers with performances considerably better than current state of the art in all other PC based (and non-PC based) structures.

II.E Integrated photonic crystal based interferometers

If two light beams pass through a dispersive medium, they can form interference patterns on a detection plane as illustrated in Figure 11. This brings about the possibility to estimate the input spectrum by looking at the output interference pattern. Also, since this device is an interferometer, any phase changes manifest itself as a change of the output interference pattern for any incident wavelength.

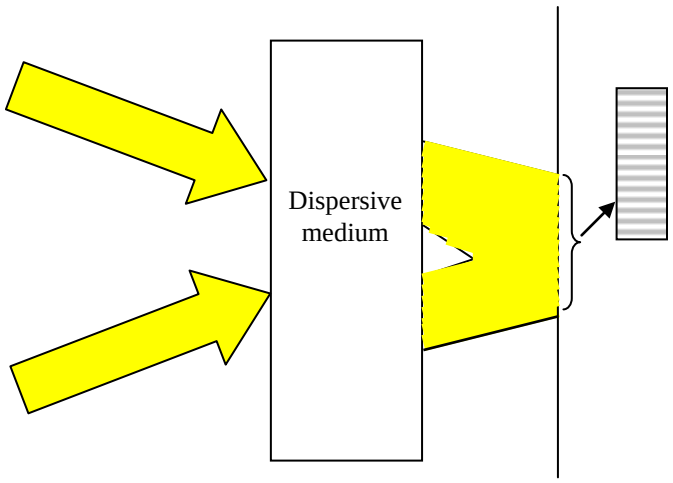

Figure 11: Schematic of an on chip interferometer

In order to have high sensitivity, we need a super dispersive medium. A good candidate is photonic crystal. Photonic crystals provide a broad range of dispersive properties. Also, they can be easily implemented on chip using different materials and on different platforms such as SOI.
A simple arrangement in which photonic crystals can be used is Young's interferometer as shown in Figure 12. The incident light beam is divided into two paths inside the photonic crystal region and they interfere on the detection plane where they can be detected using an array of detectors.

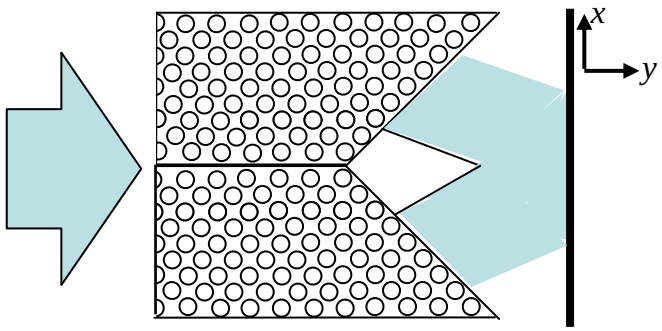

Figure 12: PC based interferometer in Young's arrangement

The output intensity can be represented by: $I_{out} \propto 1+\cos(\Delta k_x x + \Delta k_y d + \phi_0)$

The parameter $\frac{d(\Delta k_x)}{d\omega}$ is a measure of sensitivity of the interferometer. This parameter is calculated both for the PC-based interferometer and for the same structure without PC. It can be seen from Figure 13 that the sensitivity of PC-based interferometer is improved by almost an order of magnitude.

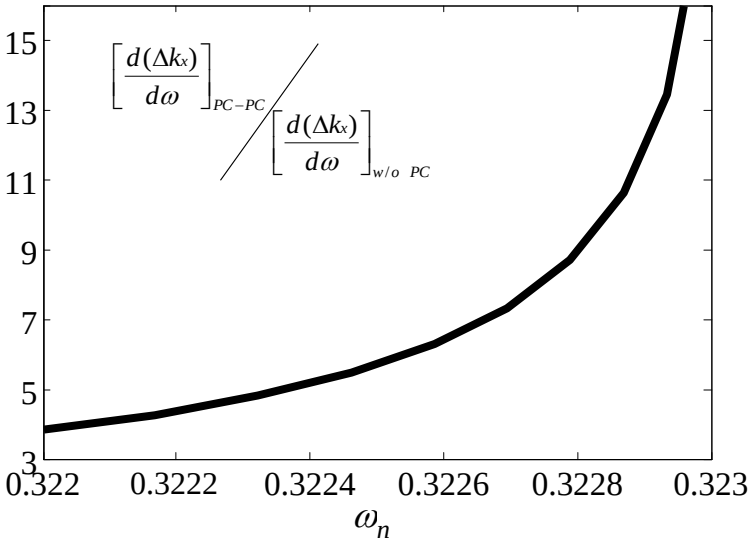

Figure 13. Relative sensitivity of the PC-based interferometer.

Photonic crystals can be used in different interferometry arrangements such as Young's arrangement, Fabry-Prot based interferometers and Wedge interferometers. These structures are capable of measuring both phase changes and input spectrums, and have potential applications in lab-on-a-chip sensing.

These interferometers have been fabricated and results reported in literature.

II F. High transmission, low dispersion PCW bends

PCW can offer a viable and compact alternative to other integrated optic platforms, but there are challenges associated with it. One of the challenges is the non optimal performance of PCW bends in the frequency range of interest. Most of the previous work on PCW bends has concentrated on improving just the transmission and dispersive behavior has been largely overlooked. We have designed PCW bends keep both their transmission and dispersion behavior in mind. We have used the mode matching technique to design large bandwidth bends with high transmission and low dispersion.

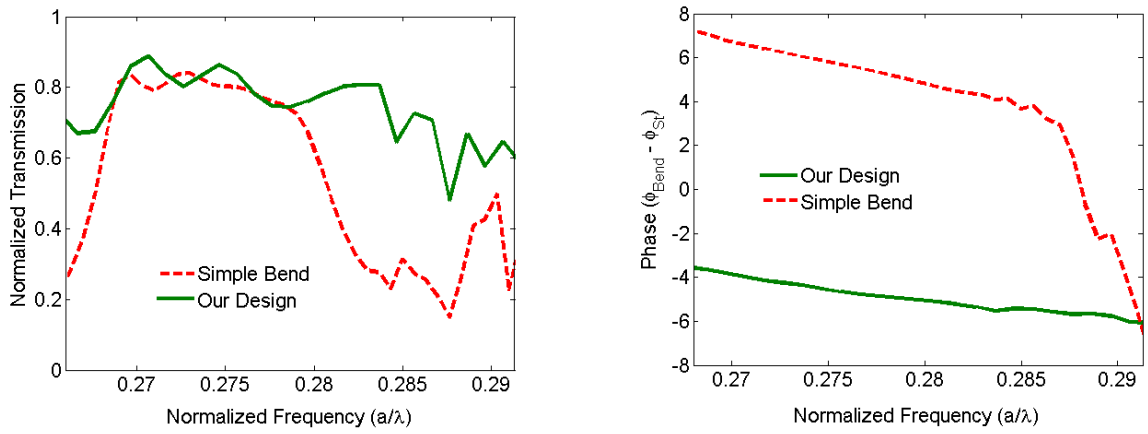

Figure 14. Comparison of transmission (left) and phase response (right) of our designed bends (green solid curve) with a simple bend (red dashed curve).

These results have already been report in literature. We have also fabricated and characterized the performance of these bends and the results will be reported in a journal paper shortly.

II G. Efficient absorption of low group velocity modes in PCW simulations

Photonic crystal waveguides are unique in that they offer low group velocity modes. These low group modes of the PCWs have application in optical delay lines and non-linear optics. For modeling such structures, normal perfectly matched layers (PMLs) are not efficient in absorbing low group velocity modes due to their homogeneous nature. Although the group velocity in the homogeneous PML region can be made arbitrarily slow by choosing appropriate permittivity and permeability but it won't have the dispersion to absorb the incoming light from a PCW, which has considerable group velocity dispersion for even a small bandwidth signal. By extending the photonic crystal (PC) region into the PML, we can absorb high group velocity signals efficiently. To absorb wide bandwidth signals efficiently we design a pre-condition PCW region before our PML in which we match our incoming signal of low group velocity to high group velocity modes of the PML PCW region. This has allowed us to reduce the reflections from PML by 10 dB in the high group velocity region and even more in low group velocity region. We call this PML as adiabatically tapered PML (AT-PML). The results are shown in the following figure. We have already submitted a journal paper on this work and it should be appearing in near future.

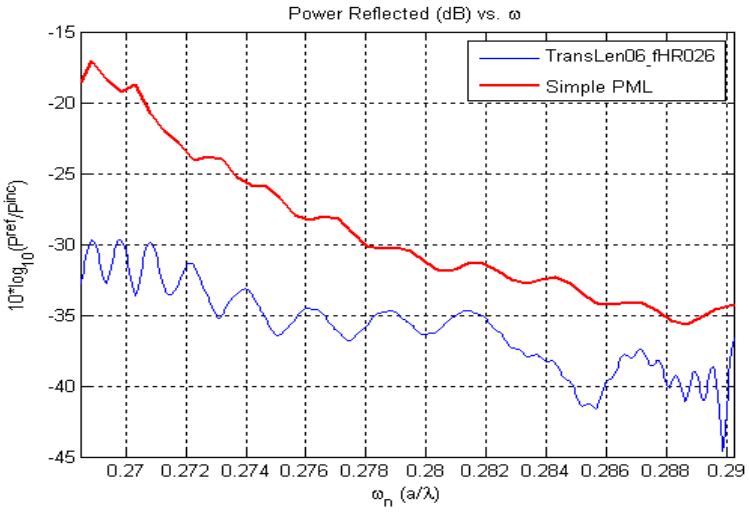

Figure 15. Comparison of reflections from homogenous PML (red) and adiabatically tapered PML (blue) shows considerable improvement (i.e., reflection reduction) in the modeling of PCWs.

II H. Refractive index sensing using slow light PCWs

PCWs have interesting applications in the slow light regime. Operating at slow light allows enhanced light matter interaction due to enhanced light intensities. Also, at slow group velocities the field overlap of the mode with air hole or a material in the air holes is larger than at large group velocities, and hence PCW operating at slow group velocities are good candidates for sensing applications. We have recently demonstrated refractive index sensing using PCW in their slow light regime. For ease of detection we have used Mach Zahnder interferometer in an unbalanced configuration. This configuration results in spectral fringes. These spectral fringes move when the refractive index of the cladding changes. By using interferometric sensors rather than resonance based sensors we obtain a larger dynamic range and tunable sensitivity, with sensitivity tuned by changing the length of the sensing region. We have shown a factor of 8 improvements over a ridge waveguide based sensor and our shift sensitivity (shift in spectral fringes as a function of refractive index of the cladding) is considerably higher than resonance based sensors using microring resonators. Experimental results of our fabricated RI sensors are shown in Figure 16. We have presented our results in a couple of conferences and are in the process of writing a journal paper on this work. Theoretically the improvement in performance over a ridge waveguide based sensor is almost three orders of magnitude. With better fabrication we should be able to probe lower group velocities and hence we expect better improvement factors in future.

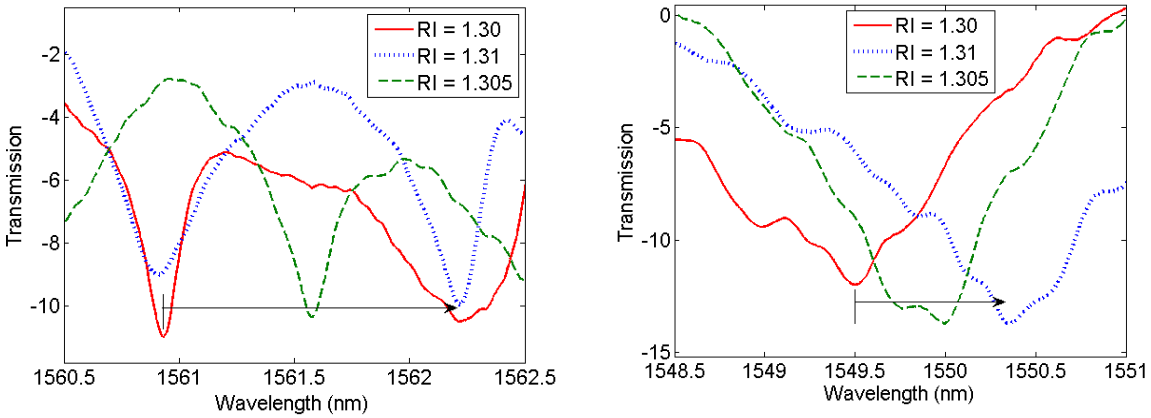

Figure 16. Characterization results for unbalanced Mach-Zahnder interferometer based PCW (left) and a ridge waveguide (right) sensor. Shown is the shift in spectral dip as we change the index of the surrounding medium.

III. Publications and Presentations

While some of the journal papers based on our works in this program have yet to appear as they are still being prepared. During the course of this program we have written many journal papers and have also presented our work at major conferences. Following is a list of some of the publications/presentations resulting from our work. An exhaustive list of work can be obtained through Dr. Adibi

III.A. Journal papers

1. B. Momeni, A. A. Eftekhar, and A. Adibi, "Effective impedance model for analysis of reflection at the interfaces of photonic crystals," Optics Letters 32, 778-780 (2007).

2. B. Momeni, M. Chamanzar, E. Shah Hosseini, M. Askari, M. Soltani, and A. Adibi, "Strong angular dispersion using higher bands of planar silicon photonic crystals," Opt. Express **16**, 14213-14220 (2008).

3. A. H. Atabaki, E. Shah Hosseini, B. Momeni, and A. Adibi, "Enhancing the guiding bandwidth of photonic crystal waveguides on silicon-on-insulator," submitted to Opt. Lett.

4. M. Chamanzar, B. Momeni, and A. Adibi, "Compact on-chip interferometers with high spectral sensitivity," Opt. Lett., **34**, 220-222 (2009).

5. B. Momeni, E. Shah Hosseini, M. Askari, M. Soltani, J. Huang, and A. Adibi, "Integrated photonic crystal spectrometers for sensing applications," Opt. Communic., **282**, 3168-3171 (2009)

6. B. Momeni, S. Yegnanarayanan, M. Soltani, A. A. Eftekhar, E. Shah Hosseini, and A. Adibi, "Silicon nanophotonic devices for integrated sensing ," J. Nanophotonics., **3**, 031001 (2009)

7. B. Momeni, and A. Adibi, "Adiabatic matching stage for coupling of light to extended Bloch modes of photonic crystals," Applied Phy. Lett., **87**, 171104 (2005).

8. M. Askari, B. Momeni, M. Soltani, and A. Adibi, "Systematic design of wide-bandwidth photonic crystal waveguide bends with high transmission and linear dispersion," J. of Lightwave Technol. **28**, 1707-1713 (2010).

9. M. Askari, B. Momeni, C. M. Reinke, and A. Adibi, "Absorbing boundary conditions for low group velocity electromagnetic waves in photonic crystals," Applied Optics, submitted.

III.B. Conference presentations

1. M. Chamanzar, B. Momeni, and A. Adibi, "Highly Sensitive Compact On-Chip Micro-Interferometers," Integrated Photonics and Nanophotonics Research and Applications (IPNRA), Boston, MA, July 2008.

2. E. Shah Hosseini, S. Yegnanarayanan, and Ali Adibi, "Ultra-High Quality Factor Silicon Nitride Planar Microdisk Resonators for Integrated Photonics in the Visible Range," Integrated Photonics and Nanophotonics Research and Applications (IPNRA), Boston, MA, July 2008.

3. B. Momeni, M. Chamanzar, E. Shah Hosseini, M. Askari, M. Soltani, and A. Adibi Implementation of high resolution planar wavelength demultiplexers using strong dispersion in photonic crystals," Conference on Lasers and Electro-Optics (CLEO), San Jose, CA, May 2008.

4. C. M. Reinke, A. A. Eftekhar, X. Zhang, B. Momeni, and A. Adibi, "Analysis of scattering losses in photonic crystal structures using a Green's function-based approach," Photonics West 2008, San Jose, CA, January 2008.

5. A. H. Atabaki, E. Shah Hosseini, B. Momeni, and A. Adibi, "Engineering of planar photonic crystal waveguides on silicon-on-insulator for larger guiding bandwidth," Photonics West 2008, San Jose, CA, January 2008.

6. B. Momeni, M. Chamanzar, M. Askari, M. Soltani and A. Adibi, "High-resolution compact photonic crystal devices for integrated wavelength demultiplexing," LEOS Annual Meeting, Lake Buena Vista, FL, October 2007.

7. M. Askari, B. Momeni, S. Yegnanarayanan, A. Eftekhar, and A. Adibi, "Efficient coupling of light into the planar photonic crystal waveguides in the slow group velocity regime," SPIE Photonics West, San Jose, CA, January 2008.

8. M. Askari, S. Yegnanarayanan, and A. Adibi, "Refractive index sensing using slow light in photonic crystal waveguides, " CLEO, San Jose, July, 2010.

III.C. Invited talk

1. B. Momeni, M. Chamanzar, E. Shah Hosseini, M. Askari, M. Soltani, and A. Adibi, "Design and applications of strongly dispersive photonic crystal structures," Photonics West 2008, San Jose, CA, January 2008 (invited).

2. A. Adibi, "Ultra-compact wavelength demultiplexers and spectrometers using mode engineering in photonic crystal super-dispersive structures," SPIE Optics & Photonics, San Diego, CA, August 2008 (invited).

3. M. Askari, and A. Adibi, "Wide bandwidth photonic crystal waveguide bends," SPIE Photonics West, San Francisco, CA, January 2010 (invited)